Alkalinity and nitrate dynamics reveal dominance of anammox in a hyper-turbid estuary

Mona Norbisrath[1,2], Andreas Neumann[1], Kirstin Dähnke[1], Tina Sanders[1], Andreas Schöl[3], Justus E. E. van Beusekom[1], and Helmuth Thomas[1,2]

[1]Institute of Carbon Cycles, Helmholtz-Zentrum Hereon, Geesthacht, 21502, Germany
[2]Institute for Chemistry and Biology of the Marine Environment, Carl von Ossietzky University Oldenburg, Oldenburg, 26129, Germany
[3]Department of Microbial Ecology, Federal Institute of Hydrology, Koblenz, 56068, Germany

Correspondence to: Mona Norbisrath (mona.norbisrath@gmail.com)

Abstract

Total alkalinity (TA) regulates the oceanic storage capacity of atmospheric CO_2. In heterotrophic temperate estuaries, anaerobic respiration of organic matter, e.g., by denitrification, the anaerobic reduction of nitrate (NO_3^-) to elemental nitrogen (N_2), can be an important source of TA. Anammox, in contrast, yields N_2 as its terminal product via comproportionation of ammonium (NH_4^+) and nitrite (NO_2^-); however, this occurs without release of TA as a byproduct. In order to investigate these two nitrate / nitrite respiration pathways and their resulting impact on TA generation, we sampled the highly turbid estuary of the Ems River, discharging into the North Sea in June 2020. We sampled a transect from the Wadden Sea to the upper tidal estuary, fluid mud for incubation experiments, and five vertical profiles during ebb tide in the hyper-turbid tidal river. The data reveal a strong increase of TA and DIC in the tidal river, where stable nitrate isotopes indicate water column denitrification as the dominant pathway. However, in the fluid mud of the tidal river, the TA data and the N_2 incubation experiments imply only low denitrification rates, with the majority of the N_2 being produced by anammox (> 90 %). The relative abundances of anammox and denitrification, respectively, thus exert a major control on the CO_2 storage capacity of adjacent coastal waters.

1 Introduction

Global and climate change leads to profound challenges in the coastal zone. Amongst these are respective impacts on the CO_2 storage capacity of the coastal seas, which has gained increasing scientific attention (Burt et al., 2016;Reithmaier et al., 2020;Thomas et al., 2009;2007;Van Dam et al., 2021;Voynova et al., 2019). In contrast to the open ocean, the carbon cycle in coastal oceans generally exhibit much higher dynamics (Borges et al., 2005;Frankignoulle et al., 1998;Thomas et al., 2009;2004). These dynamics are even more accentuated in estuaries that are subject to human interventions like dredging, damming, nutrient inputs, or transportation.

Continental and intertidal estuaries, such as the Ems Estuary (German-Dutch border) on which we focus in this study, are the interface between coast and land. The Ems is exposed to high nutrient inputs, hosts high suspended particulate matter (SPM)

concentrations (Van Beusekom and De Jonge, 1998), and has shown already active nitrogen alternation (Sanders and Laanbroek, 2018;Schulz et al., 2022) which makes it a perfect natural laboratory to study the linkage of total alkalinity (TA) and nitrate respiration.

One of the largest impacts on the ocean is the increasing anthropogenic CO_2 content in the atmosphere, part of which is absorbed by the ocean. The ocean's TA, buffers the ocean's acidification by the absorbed weak acid CO_2. TA in turn is either generated by chemical rock weathering (Berner et al., 1983;Meybeck, 1987;Suchet and Probst, 1993), or metabolically by various anaerobic or inorganic pathways releasing TA in various stoichiometries (Brewer and Goldman, 1976;Chen and Wang, 1999;Hu and Cai, 2011;Wolf-Gladrow et al., 2007) e.g., by denitrification.

As a CO_2 buffer, the coastal zone is exposed to high agricultural nutrient loads, which can lead to coastal eutrophication, foster primary production, and increase seasonal anoxia (Große et al., 2016;Howarth et al., 2011;Nixon, 1995). High nutrient loads also trigger nitrate respiration pathways, such as denitrification and anammox. During denitrification, nitrate (NO_3^-) is reduced to nitrous oxide (N_2O) and then finally to dinitrogen gas (N_2). During denitrification, anaerobic bacteria, i.e., denitrifiers, use NO_3^- as terminal electron acceptors and irreversibly generate TA in a ratio of 0.9 (Chen and Wang, 1999).

Unlike denitrification, anammox, the anaerobic ammonium oxidation, has no effect on TA (Middelburg et al., 2020). Here, the electron donor ammonium (NH_4^+) is oxidized with the electron acceptor nitrite (NO_2^-) to release N_2 (Meyer et al., 2005;Mulder et al., 1995;Thamdrup and Dalsgaard, 2002).

In light of governing the CO_2 buffer capacity of coastal oceans, the proportions in which anammox and denitrification serve to reduce NO_2^- or NO_3^- play a crucial role. In this study, we investigate nitrate respiration pathways and combine nitrate respiration rates and processes with carbon and nitrogen cycle observations. The combination of TA generation and nitrate removal allows us to a) shed light on the interaction between TA and nitrate or nitrite respiration pathways, and b) aids to disentangle anammox and denitrification in the estuary. To the best of our knowledge, this is one of the first studies in which TA generation is used as a tool to discriminate and underpin calculated potential N_2 production pathways. Based on TA generation and an isotope pairing approach, we find that anammox dominates in this heterotrophic environment.

2 Materials and methods

2.1 Study site and water sampling

The Ems Estuary is located at the border between Netherlands and Germany. Including the outer estuary, it is approximately 100 km long, starts at the weir in Herbrum and discharges in the Wadden Sea (Fig. 1), which connects to the North Sea (NE Atlantic shelf). The tidal range increased from 2 m to 3.6 m (1950-2010) in the upstream estuary (De Jonge et al., 2014;van Maren et al., 2015). The Ems Estuary permanently underlies natural and anthropogenic pressures. Due to estuarine and riverine sea ports and the German shipyard in Papenburg, the accessibility for large ships is needed. Channel deepening and dredging activities that already started in the 1950s in the outer estuary and in the 1980s in the tidal river lead to hyper-turbid conditions (De Jonge et al., 2014). This topographic change results in increasing loads of marine suspended particulate matter (SPM),

which accumulate in the upstream estuary and cause high oxygen demand for bacterial degradation and remineralization (Jonge, 1983;De Jonge et al., 2014). Another indirect sink for oxygen are the high loads of fertilizer, which also increase
65   eutrophication and oxygen consumption (Howarth et al., 2011;Nixon, 1995;Van Beusekom et al., 2019).

A special characteristic of the present Ems Estuary is the section of fluid mud in the bottom layers of the tidal river that reaches on average the upper 40 km of the estuary (Becker et al., 2018;De Jonge et al., 2014;Talke et al., 2009). Fluid mud is highly concentrated in SPM and separated from the overlying pelagic water.

Transect water samples were collected on board the RV *Ludwig Prandtl* (LP20200602) along the salinity gradient, starting
70   from the North Sea northwest of the barrier island Borkum, to the weir in Herbrum during ebb tide on June 11th and 12th 2020 (Fig. 1). We continuously collected surface water samples (1.2 m depth) using a bypass from the onboard flow-through FerryBox system (Petersen et al., 2011), which provided important physical parameters such as salinity, temperature, and oxygen. For initial river values, we took one sample upstream of the weir. A special focus is placed on the area of the tidal river that reaches from the Weir Herbrum (at Ems stream km -14.1) downstream to Ems stream km 36 (last station upstream
75   the Dollart).

For incubation experiments, we sampled fluid mud with the bottom water sampler at two stations (Ems stream km 7.8 and km 17.3, named as station 714 & 715, respectively) at ebb tide on June 11th 2020.

Additionally, vertical profile (VP) samples during ebb tide were provided by the German Federal Institute of Hydrology (Bundesanstalt für Gewässerkunde - BfG). These samples were taken at Ems stream km 7.2 on June 17th, six days after the
80   surface transect sampling. Samples were taken from high tide to low tide, with vertical samplings started at 11:01 (named as VP1), 12:29 (VP2), 13:58 (VP3), 15:00 (VP4), and 18:22 (VP5). Vertical profiles were measured at various depths, either directly with probes (salinity, temperature, oxygen, depth), or indirectly by discrete water samples (nutrients, isotopes). The deepest samples were always taken 0.5 m above the bottom. Oxygen concentrations, salinity, temperature and depth were measured in situ with an YSI6660 EXO2 multi parameter probe. Suspended particulate matter was determined gravimetrically
85   (DIN 38 409-H2). Therefore, water samples of 0.2 to 1 L volume were filtered through pre-sealed Whatman filters, dried at 550 °C, and weighed.
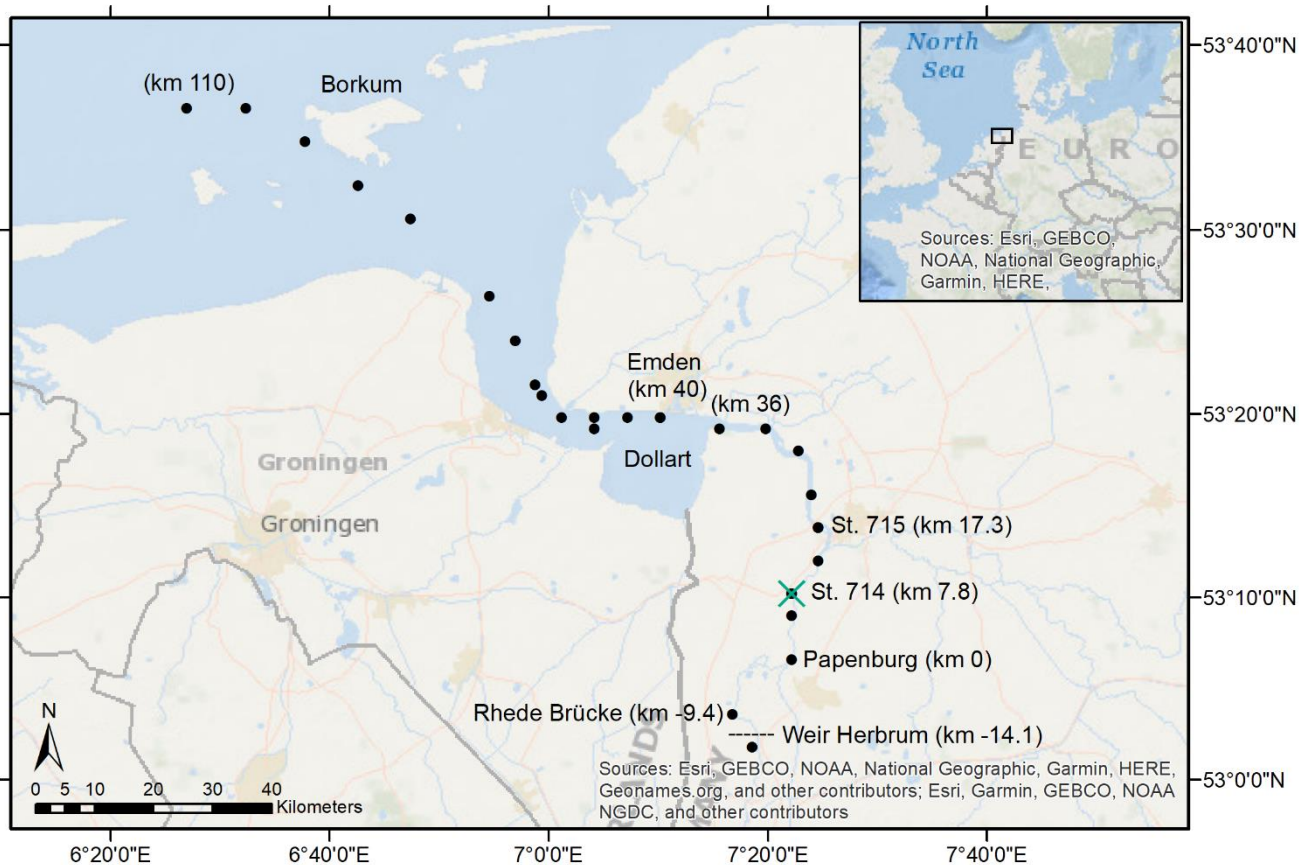
Figure 1. Sampling stations in the Ems Estuary in June 2020. The vessel based transect ended in Papenburg, corresponding to Ems stream km 0. We took samples at Rhede Brücke and upstream Weir Herbrum from shore. The transect sampling stations are marked with the black dots, the vertical profile station at Ems stream km 7.2 with the green cross. The tidal river reaches from the Weir Herbrum river downstream to Ems stream km 36 (the last station upstream the Dollart).

2.2 TA and DIC

For total alkalinity (TA) and dissolved inorganic carbon (DIC) measurements along the transect, we sampled 300 mL water with overflow into BOD (biological oxygen demand) bottles and preserved them with 300 μL saturated mercury chloride ($HgCl_2$) to stop biological activity. BOD bottles were closed air bubble free with ground-glass stoppers coated in Apiezon® type M grease, and secured with plastic caps. The samples were stored cool in the dark.

The parallel analyses of TA and DIC were carried out by using the VINDTA 3C (Versatile INstrument for the Determination of Total dissolved inorganic carbon and Alkalinity, MARIANDA - marine analytics and data), which measures TA by potentiometric and DIC by coulometric titration, respectively (Shadwick et al., 2011). To ensure a consistent calibration at both measurements, we used Certified Reference Material (CRM batch # 187) provided by Andrew G. Dickson (Scripps Institution of Oceanography).

2.3 Nutrients

Along the transect, water for nutrients was sampled with the FerryBox bypass, filtered over pre-combusted (4h, 450 °C) GF/F filter, and stored frozen in 3 x 15 mL Falcon tubes.

105 The nitrate concentrations of the transect samples were analyzed with a continuous flow automated nutrient analyzer (AA3, SEAL Analytical) and a standard colorimetric technique (Hansen and Koroleff, 2007). Samples were analyzed in triplicate. The water for nutrient samples of the vertical profiles was pumped onboard, centrifuged and the supernatant was measured back ashore. Samples of the vertical profiles were analyzed for nitrate, nitrite and ammonium with a continuous flow analyzer (Skalar SC 13900) at the German Federal Institute of Hydrology (BfG). The automated procedure for determining ammonia

110 is based on the modified Berthelot reaction (Krom, 1980). The determination of nitrate and nitrite is based on the Griess reaction and measured after Kroon (1993).

For calculating horizontal nutrient consumption or production rates, we used the following equation:

$$rate = \left(\frac{\Delta_{conc.}}{\Delta_{dist.}}\right) * \Delta_{time} \tag{1}$$

where the differences Δ of nutrient concentrations (Δ_{conc}), time (Δ_{time}), and altitude, i.e., distance to the bottom (Δ_{dist}) between

115 the two deepest depths of the vertical profiles VP4 and VP5 were used to detect a nutrient consumption or production during the end of ebb tide.

2.4 δ^{15}N and δ^{18}O stable isotopes

Along the transect, water for stable nitrate isotopes was sampled with the FerryBox bypass, filtered over pre-combusted (4h, 450 °C) GF/F filter, stored frozen in 100 mL PE bottles (acid-washed with 10 % HCl overnight), and analyzed by Schulz et

120 al. (2022). Vertical profile water samples provided by BfG were also analyzed for stable nitrate isotopes by using the denitrifier method (Casciotti et al., 2002;Sigman et al., 2001). Briefly, the denitrifier method is based on a bacterial strain of *Pseudomonas aureofaciens* (ATCC#13985) that lacks nitrous oxide reductase activity and reduces nitrate and nitrite only to nitrous oxide and not further to N_2. The product is then measured using an isotope mass spectrometer (Delta Plus XP, Fisher Scientific) coupled to a GasBench II.

125 In order to support the identification of pathways (e.g., Kendall et al., 2007), we calculated isotope effects (ε) for the deepest depth of the two last vertical profiles (VP4 & VP5), which showed the strongest nitrate decrease. We used an open-system approach assuming a steady state, and continuously supplied and partially consumed substrate, resulting in a linear relationship between the isotope values and the remaining fraction (*f*). The slope of the regression line corresponds to the isotope effect (ε), and (*f*) to the remaining fraction of substrate at time of sampling (Sigman et al., 2009).

130 $$\varepsilon_{substrate} = \frac{\delta^{15}N \ (or \ \delta^{18}O) \ substrate - \delta^{15}N \ (or \ \delta^{18}O) \ initial}{(1-f)} \tag{2}$$

where the $\delta^{15}N \ (or \ \delta^{18}O)_{substrate}$ is the delta value at the time of sampling, and $\delta^{15}N \ (or \ \delta^{18}O)_{initial}$ is the initial delta value at the surface in the beginning of each vertical sampling.

$$f = \frac{[1 - C]}{[C_{initial}]} \qquad \qquad (3)$$

where C is the concentration of nitrate at time of sampling and $C_{initial}$ is the initial nitrate concentration at surface, in the beginning of each vertical sampling.

In addition, we measured stable isotopes of nitrite after the method by Böhlke et al. (2007), by using a bacterial strain of *Stenotrophomonas nitritireducens* (ATCC#BAA-12) that reduces nitrite to nitrous oxide. We used these data in order to quantitatively identify whether nitrite stems from organic matter (OM) and ammonium by nitrification, or from nitrate by denitrification.

2.5 Incubations for N_2 determination and TA generation

Observed carbon and nitrogen data of incubation experiments in the fluid mud were combined to shed light on the interaction between TA generation and N_2 production in the upper tidal river of the Ems Estuary.

In order to determine the N_2 production and to detect the different isotopic N_2 species $^{28}N_2$, $^{29}N_2$ and $^{30}N_2$ in the bottom water of the Ems Estuary, we combined the N_2:Ar ratio measurements using the MIMS (Membrane Inlet Mass Spectrometer) (Kana et al., 1994) with the expanded (Risgaard-Petersen et al., 2003) isotope pairing technique (IPT) (Nielsen, 1992). The addition of the IPT allowed us to discriminate between denitrification and anammox as both pathways producing N_2 (Risgaard-Petersen et al., 2003) and calculate potential N_2 production rates.

2.5.1 Incubation set-up

For the incubation experiment, we took fluid mud samples with a bottom water sampler at ebb tide at two stations low in surface oxygen (St. 714: ~ 64 µmol O_2 L^{-1}; St. 715: ~ 91 µmol O_2 L^{-1}), and filled them in one-liter Schott bottles without headspace. To get initial concentrations, we took samples before adding the ^{15}N-NO_3^- tracer, with 137 µmol NO_3^- L^{-1} at station 714, and 144 µmol NO_3^- L^{-1} at station 715. After adding 30 mL 10 mM ^{15}N-NO_3^- tracer ($\geq$ 98 atom % ^{15}N) stock solution, we closed the bottle bubble free with a rubber stopper for gentle mixing. For sampling, the rubber stopper was prepared with two cut pipettes; one to fill the exetainer (12 mL Labco Exetainer®), the other one to replace the outflowing water by air. The incubation ran in parallel replicates in exetainers for 1, 4, 18, 28 and 43 hours in total. The incubation time was adjusted to a parallel oxygen measurement by using a fiber-optic sensor and FireSting set up (PyroScience GmbH) that started an hour after labelling (at time step t1). At time step t1, the oxygen concentrations of the incubations were ~ 11 µmol O_2 L^{-1} at station 714, and ~ 64 µmol O_2 L^{-1} at station 715, providing almost anoxic conditions. To inhibit the incubation and preserve the samples, we injected approximately 100 µL 50 % zinc chloride ($ZnCl_2$) through the septum into each exetainer.

For the carbon, i.e., TA generation data, we sampled two BODs out of the N_2 incubation experiment of both incubation stations for estimating TA generation rates in the fluid mud. The TA and DIC sampling and analyses were performed in the same way as described above (2.2). However, we preserved the first BOD directly after sampling (0h) to get start values, i.e., initial

concentrations of TA and DIC, and the second BOD after 43 hours (43h) at the end of the incubation, to ensure a comparison between the start and end point of TA and DIC along the incubation (BOD incubation).

2.5.2 N_2:Ar analysis with the MIMS

Samples for N_2 measurements were analyzed with a GAM-200 Quadrupol Mass Spectrometer (InProcess Instruments), which was connected to an in-house-built flow-through membrane inlet and a cryo-trap (liquid N_2) to remove water vapor from the sample stream. The stable nitrogen isotopes were measured at mass to charge ratio (m/z) 28 for $^{28}N_2$, at m/z 29 for $^{29}N_2$, and m/z 30 for $^{30}N_2$, respectively. Argon was measured as the inert reference at m/z 40 (Kana et al., 1994). The integration time was 0.5 s. For calculating the N_2 concentrations, we used equilibrium values calculated after Hamme & Emerson (2004). We calibrated the sample measurements by using 3 different seawater standards (salinity of 20, 30, and 40) and MilliQ (0 salinity) equilibrated at 5 °C.

We calculated the various produced parameters based on the equations by Risgaard-Petersen et al. (2003) in which D28 (denitrification of $^{28}N_2$) was calculated with their Eq. 17, D29 with their Eq. 16, D30 equals $p^{30}N_2$ (the produced $^{30}N_2$ amount), A28 with their Eq. 18, A29 with their Eq. 19, P14 with their Eq. 4, and r14 equals the ratio of measured initial $^{14}N\text{-}NO_3^-$: added $^{15}N\text{-}NO_3^-$.

2.6 TA and N_2 production coupling

In order to shed light on the interaction between TA and denitrification, we compared the TA generation of the BOD incubation of each station with the average N_2 production per station. We used the average TA increase of the BOD incubations, converted it to the equivalent maximum possible TA generation due to denitrification, and subtracted it from the total N_2 production. To equalize TA generated by denitrification, we calculated the TA gain as the corresponding amount of nitrogen. For this, we used the ratio of 0.9 for TA generation by denitrification (Chen and Wang, 1999) and subtracted it from the total N_2 production (Table 2). We assumed that the remaining produced N_2 would be produced by anammox. By using this approach, we can estimate and prove the results of the IPT calculation, and discriminate potential N_2 production pathways by denitrification and anammox.

2.7 Data analysis

The data analyses were performed by using RStudio Version 1.3.1073 © 2009-2020 RStudio, PBC and the R packages "tidyverse", "ggplot2", "ggpmisc", and "lmodel2".

3 Results

 3.1 Carbon status in the estuary

The distribution of total alkalinity (TA) and dissolved inorganic carbon (DIC) ranged from 2357 µmol TA kg^{-1} and 2541 µmol DIC kg^{-1} upstream of the weir in Herbrum, over 2487 µmol TA kg^{-1} and 2671 µmol DIC kg^{-1} directly after the weir, to a maximum of 2662 µmol TA kg^{-1} and 2858 µmol DIC kg^{-1} at Ems stream km 7.8. After the maximum, TA and DIC decreased to values around 2394 µmol TA kg^{-1} and 2176 µmol DIC kg^{-1} in the North Sea (Fig. 2a). We observed maximum TA and DIC

195 concentrations in the tidal river, and in a range between salinity 0 and 5. From the weir to the TA maximum at Ems km 7.8 (five sampling points), we observed a TA gain of 305 µmol kg^{-1}.

The concurrent range of salinity varied from fresh water (0.5 salinity) to a salinity of 32.31 in the North Sea. The temperature varied between 18 °C and 15 °C along the entire transect from the weir in Herbrum (fresh water) downstream to the North Sea. In the outer estuary between Ems stream km 37 and 110 (salinity > 15), TA and DIC slightly decreased with increasing

200 salinity, indicating the stronger impact from the Ems also on downstream regions (Fig. 2a,b). The almost linear behavior of DIC and TA indicated that ongoing processes act proportionally on both species (Fig. 2c). We observed a clear deviation from linearity upstream of Ems stream km 36, i.e., in the tidal river (Fig. 2d). The $R^2 = 0.49$ indicated that around 50 % of the DIC can be explained with TA, the remaining indicating other, likely oxic processes being responsible for the DIC increase. The DIC excess in the surface water of the tidal river indicated OM respiration (Wang et al., 2016) with high CO_2 generation (Fig.

205 2d).
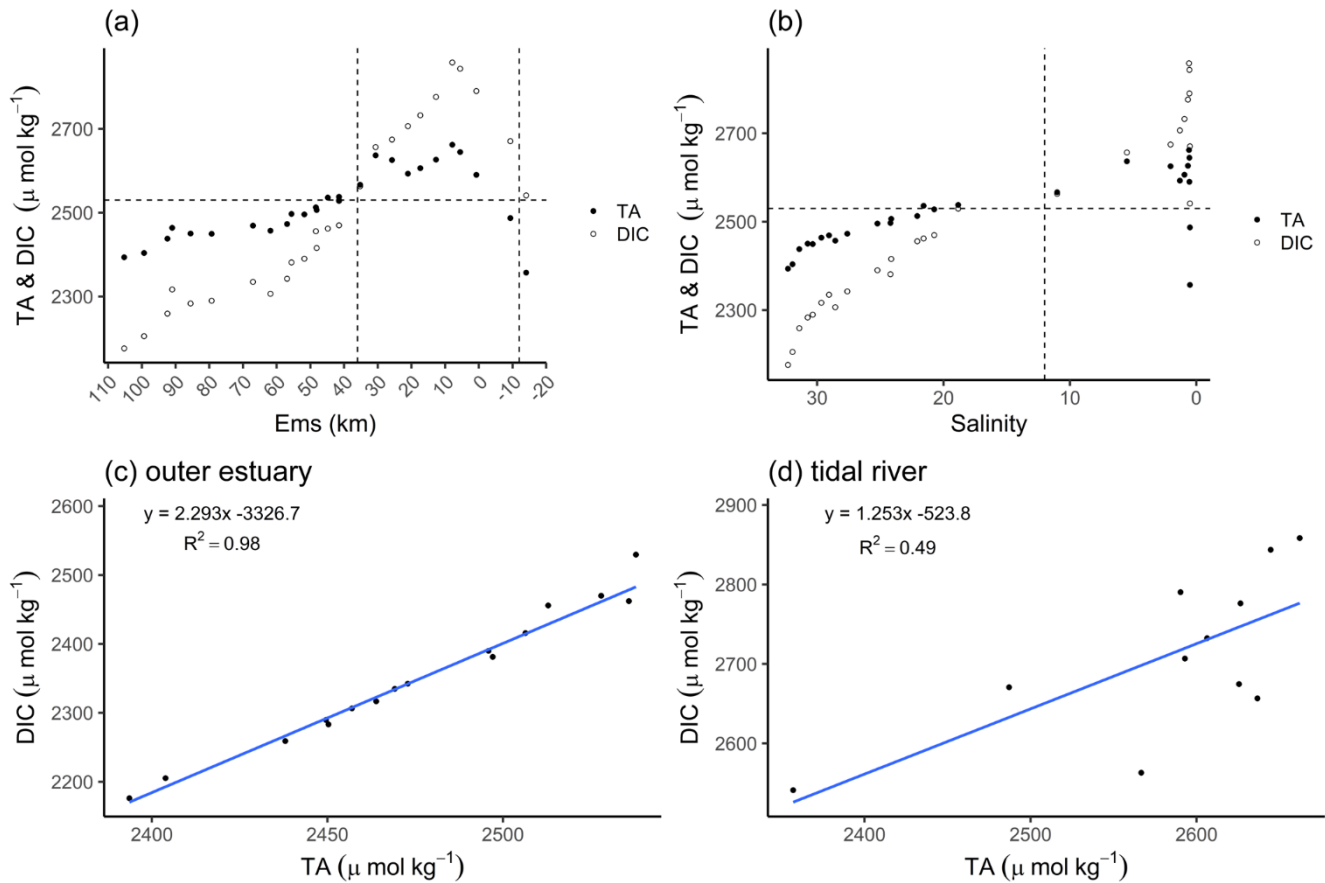
Figure 2. Total alkalinity (TA) and dissolved inorganic carbon (DIC) concentrations. The TA (black dots) and DIC (white dots) distribution is shown along the Ems Estuary in (a) stream kilometer and (b) salinity. a) The Ems stream km 110 is located around the barrier island of Borkum (North Sea), and the Ems stream km -20 is the area upstream the Weir Herbrum. The area between the weir and Ems stream km 36 is named as tidal river and visualized within the two vertical dashed lines. b) In the salinity plot, the tidal river is on the right side of the vertical dashed line between salinity 0 and 12. The plots in the second row show the relation between TA and DIC of the transect samples in c) the outer estuary from Borkum to Ems stream km 36, and in d) the tidal river.

3.2 Nitrate assessment

3.2.1 Along the estuary

In a recent study, Schulz et al. (2022) identified a dominance of denitrification with nitrification as an additional contributor in our focus area, the tidal river. They found $\delta^{15}N$ values between 15 and 30 ‰ and suggested that these were caused by denitrification as the dominant process according to Kendall et al. (2007), visualized in Fig. 3a. Here, we can further distinguish the tidal river in two zones, in the upper tidal river (upstream the weir to Ems stream km 8) and in the lower tidal river (downstream Ems stream km 8 to Ems stream km 36). By using the data of Schulz et al. (2022), we observed a strong

220 enrichment in the delta values in the upper tidal river. Concurrently, we observed a maximum nitrate (NO_3^-) concentration upstream from the weir in the riverine fresh water with 182 µmol NO_3^- L^{-1} decreasing downstream to 149 µmol NO_3^- L^{-1} at Ems km 7.8. This indicated a NO_3^- loss of 32 µmol L^{-1} in the upper tidal river where TA had the strongest increase towards the maximum suggesting denitrification as the nitrate respiration pathway. In the lower tidal river, a mixed signal of denitrification and nitrification is visible. The lighter delta values and the slightly increasing nitrate concentrations from Ems

225 km 17 downstream, indicated the occurrence of nitrification. In the salinity gradient, nitrate decreased to a common low marine concentration in the North Sea (Fig. 3a). Using the delta values, we calculated the slope of 0.485 between $\delta^{18}O$ and $\delta^{15}N$ ($\delta^{18}O:\delta^{15}N$) in the tidal river (Fig. 3b), which comes very close to the slope of 0.5 (Kendall et al., 2007;Schulz et al., 2022) and supports the relevance of denitrification.
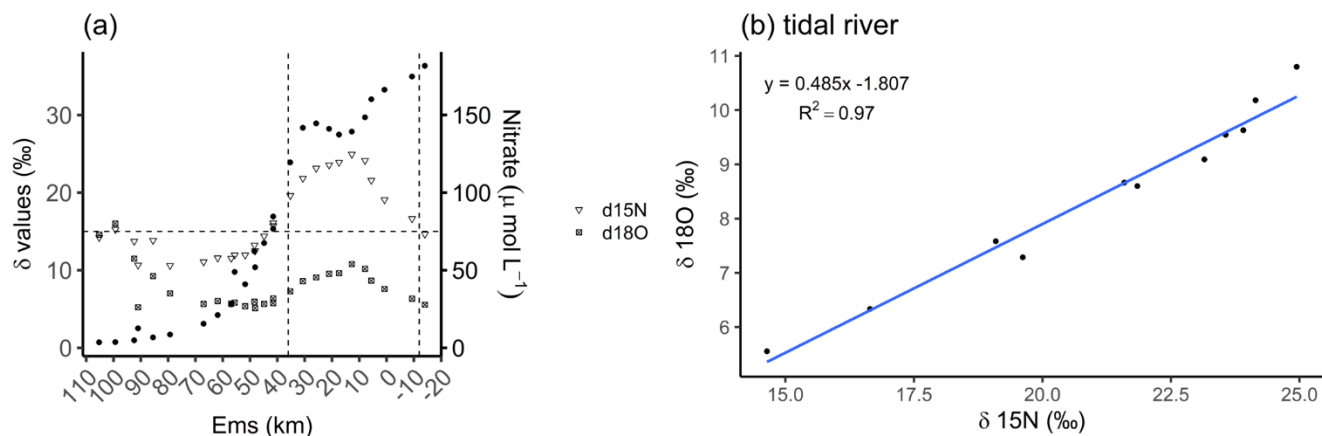
230

Figure 3. Nitrate based species distribution. a) The delta values of the nitrate stable isotopes $\delta^{15}N$-NO_3^- (inverted triangle) and $\delta^{18}O$-NO_3^- (crossed square) and the nitrate concentration (filled dots) along the Ems Estuary stream kilometer. The Ems stream km 110 is located around the barrier island of Borkum (North Sea), and the Ems stream km -20 is the area upstream the Weir Herbrum. The area between the weir and Ems stream km 36 is named as tidal river and visualized within the two vertical dashed lines. b) The relationship between nitrate stable

235 isotopes $\delta^{18}O$ and $\delta^{15}N$ in the tidal river (weir to Ems stream km 36). Data are from Schulz et al. (2022) who measured and analyzed the samples and data.

3.2.2 Vertical profiles

Six days after the cruise, samples of five vertical profiles (VP1 - VP5) were taken in the tidal river at Ems stream km 7.2 on June 17th during ebb tide. The water temperature varied between 19.5 and 21.3 °C and decreased with increasing depths (Fig.

240 4h). In the fresh water, the salinity varied slightly between 0.41 and 0.45 (Fig. 4i).

The vertical differences in SPM lead to differences in density, which causes the occurrence of vertical layering of the water masses. The SPM reached very high concentrations of above 40 g L^{-1} near the bottom, indicating that the fluid mud layer in the deepest 2 m is clearly separated from the overlying water (Fig. 4f). The separation of the water masses and a negligible

effect of advection velocity is supported by the difference in flow speed at surface (0.94 m sec^{-1}) and near the bottom (0.05 m

245   sec^{-1}). In VP5, the increased water levels and the increased values of temperature, salinity, and oxygen in the shallowest sampling point indicating the next upcoming high tide with water masses overflowing the bottom layers (two deepest depths / sampling points) (Fig. 4g-j).

Dual nitrate isotope values indicated strong fractionation in the deep layers, with δ^{15}N-NO$_3^-$ values varying between 15 and 30 ‰ and δ^{18}O-NO$_3^-$ values between 5 and 15 ‰ (Fig. 4a,b). We observed highest δ^{15}N-NO$_3^-$ values in the bottom water. δ^{18}O-

250   NO$_3^-$ values increased strongly with depth in the first four samplings (VP1 - VP4), but we observed a lower level of values towards the end of ebb tide. In particular, in the beginning of the upcoming high tide (VP5), the isotope values of δ^{18}O were clearly lower than during ebb tide, both from surface to bottom and during the tidal cycle.

Decreasing oxygen concentrations towards the bottom favor for denitrification with increasing depths (Fig. 4g). Anoxia in the deepest layer facilitated anaerobic metabolic pathways such as denitrification and anammox, although there may be more

255   pathways. Clearly decreasing nitrate concentrations indicate a loss of nitrate in the bottom layer during the entire ebb tide (Fig. 4c). The associated vertical profiles of nitrite and ammonium both showed an increase with depth during the ebb tide. Highest nitrite concentrations were found in bottom water (< 2 m) with values between 15 and 30 µmol NO$_2^-$ L^{-1} (Fig. 4d). Ammonium concentrations were up to 5 µmol NH$_4^+$ L^{-1} (Fig. 4e).
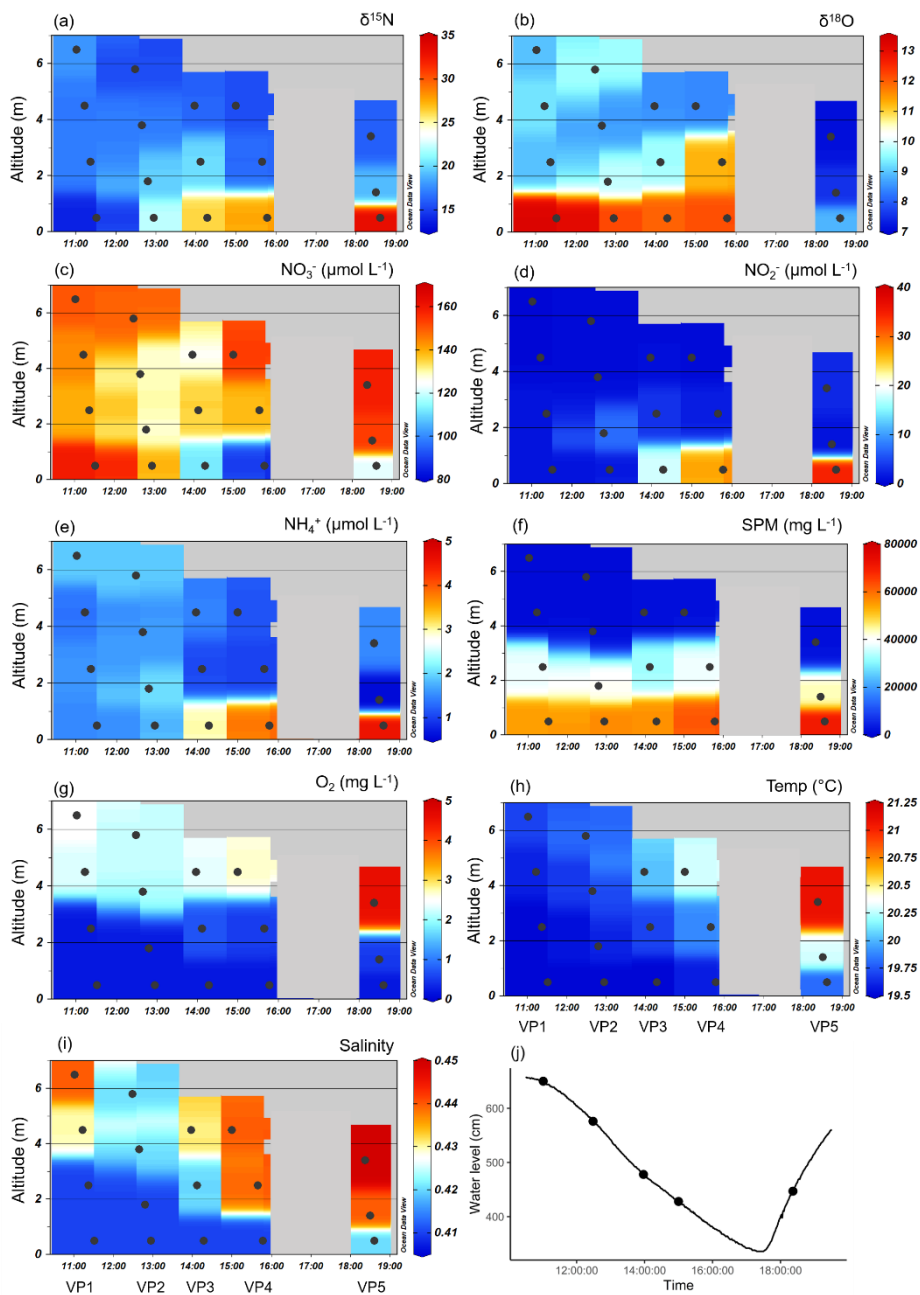
Figure 4: Vertical profiles of the various parameters during ebb tide at Ems stream km 7.2 on June 17th 2020. Delta values of the nitrate stable isotopes a) $\delta^{15}N$-NO_3^- and b) $\delta^{18}O$-NO_3^-. Associated concentrations of c) nitrate (NO_3^-), d) nitrite (NO_2^-), e) ammonium (NH_4^+), f) suspended particulate matter (SPM), g) oxygen (O_2), h) temperature, and i) salinity. Ebb tide ran from the left to the right side of each plot, indicated by decreasing water depths, which are visualized as altitude (m). The vertical samplings started at 11:01 (named as VP1), 12:29 (VP2), 13:58 (VP3), 15:00 (VP4), and 18:22 (VP5). The discrete samples are marked with dots, while the background values are gridded by

260

265

using Ocean Data View. Panel j) the tidal height as water level (line) and the vertical profile samplings (dots) observed at Weener (Ems stream km 8).

By focusing on the two deepest depths, i.e., sampling points with strongest nitrate losses of the vertical profiles VP4 and VP5, and assuming the two deepest sampling points of VP5 to be bottom layers with water masses still separated from the next upcoming high tide, we were able to calculate average horizontal nutrient loss or production rates towards the end of ebb tide (Eq. 1). Considering the differences in nutrient concentration, distance, and time, we detected an average nitrate loss rate of -4 $\mu mol\ NO_3^-\ L^{-1}\ h^{-1}$ indicating an increasing nitrate consumption with ongoing ebb tide. At the same time, we determined average nitrite and ammonium production rates of 3.0 $\mu mol\ NO_2^-\ L^{-1}\ h^{-1}$ and 0.4 $\mu mol\ NH_4^+\ L^{-1}\ h^{-1}$, so that we observed higher nitrate loss than production of nitrite and ammonium.

In addition, we calculated the isotope effects (ε) of $\delta^{15}N$ and $\delta^{18}O$ (Eq. 2, 3) as a linear regression for the two deepest depths of the vertical profiles VP4 and VP5. The isotope effects (ε) of VP4 were 34.2 ‰ for $\delta^{15}N$ and 2.5 ‰ for $\delta^{18}O$, and of VP5 70.2 ‰ for $\delta^{15}N$ and 6.4 ‰ for $\delta^{18}O$.

In order to quantitatively narrow down potential sources of nitrite in the vertical profiles, we used the stable nitrite isotopes. These $\delta^{15}N\text{-}NO_2^-$ values revealed negative values in the first half of the ebb tide (VP1 - VP3) (δ values of -6, -7 ‰, and -0.2‰), but strongly positive δ values (between 10 and 22 ‰) towards the end (VP4 - VP5).

3.3 N_2 production via denitrification and anammox

The vertical profile data suggest a strong fractionation during nitrate respiration. To quantify nitrate respiration, we determined N_2 production in an incubation experiment of fluid mud from two stations in the tidal river.

Following Nielsen (1992), we identified average potential N_2 production rates of added $^{15}N\text{-}NO_3^-$ (D15) of $25.9 \pm 6.1\ \mu mol\ N$ $L^{-1}\ h^{-1}$ and $19.3 \pm 2.5\ \mu mol\ N\ L^{-1}\ h^{-1}$ at stations 714 and 715, respectively (Table 1). At both stations, the N_2 production (D15) increased during the incubation, with a slightly higher production at the more upstream station 714 (Fig. 5a,b). For the N_2 production of in situ $^{14}N\text{-}NO_3^-$ (D14), we only detected an increasing N_2 production in the first 4 hours for station 714, and a relatively stable production over the incubation time for station 715. It appears that N_2 production from in situ $^{14}N\text{-}NO_3^-$ (D14) at station 714 increased first, and then decreased after the first hours due to depletion of the initial pool of the lighter isotope ^{14}N (Fig. 5b). Compared to station 715, we observed lower initial NO_3^- concentrations at station 714.

In order to discriminate the relative contribution of denitrification vs. anammox in the incubations, we combined the N_2:Ar ratio measurements with the IPT after Risgaard-Petersen et al. (2003). Potential N_2 production rates were calculated with the linear regression of the respective concentration as a function of time during the incubation, as indicated by the slope (Fig. 5c-h, Table 1). N_2 production increased with increasing incubation time via both anaerobic pathways. We calculated a potential N_2 production by anammox of 10.16 to 22.95 $\mu mol\ L^{-1}\ h^{-1}$, which is an order of magnitude higher than the production by denitrification (0.10 to 1.01 $\mu mol\ L^{-1}\ h^{-1}$, Table 2).

Table 1. N_2 production rates. N_2 production rates of added $^{15}N-NO_3^-$ (D15) and in situ $^{14}N-NO_3^-$ (D14) calculated after Nielsen (1992).
Denitrification rates of ^{28}N (D28), ^{29}N (D29) and ^{30}N (D30), anammox rates of ^{29}N (A29) and ^{28}N (A28), and genuine $^{14}N-N_2$ production
(P14) calculated after Risgaard-Petersen et al. (2003). The potential contribution of anammox to total N_2 production (ra) is presented as %.
Rates were calculated with the linear regression of the respective concentration as a function of the entire incubation time indicated by the
slope, which was used to calculate average values. The ra range shows the average minimum and maximum ra values of the incubation based
on the two replicates. Because we only had one initial N_2:Ar ratio for each station, we used this as a start value for the second replicate too.

Species	Unit	Station 714	Station 715
D15 N production (avg.) ± sd	$\mu mol\ L^{-1}\ h^{-1}$	25.9 ± 6.10	19.27 ± 2.5
D14 N production (avg.) ± sd	$\mu mol\ L^{-1}\ h^{-1}$	-361.64 ± 147.5	430.78 ± 52.14
D29 N production (avg.) ± sd	$\mu mol\ L^{-1}\ h^{-1}$	1.01 ± 0.09	0.37 ± 0.12
D30 N production (avg.) ± sd	$\mu mol\ L^{-1}\ h^{-1}$	0.96 ± 0.09	0.33 ± 0.11
D28 N production (avg.) ± sd	$\mu mol\ L^{-1}\ h^{-1}$	0.27 ± 0.02	0.10 ± 0.03
A29 N production (avg.) ± sd	$\mu mol\ L^{-1}\ h^{-1}$	22.95 ± 5.83	18.28 ± 2.20
A28 N production (avg.) ± sd	$\mu mol\ L^{-1}\ h^{-1}$	12.12 ± 3.08	10.16 ± 1.21
P14 N production (avg.) ± sd	$\mu mol\ L^{-1}\ h^{-1}$	25.79 ± 6.30	20.90 ± 2.60
ra range (avg. min - max)	%	$94.5 – 99.4$	$97.4 – 98.0$

305
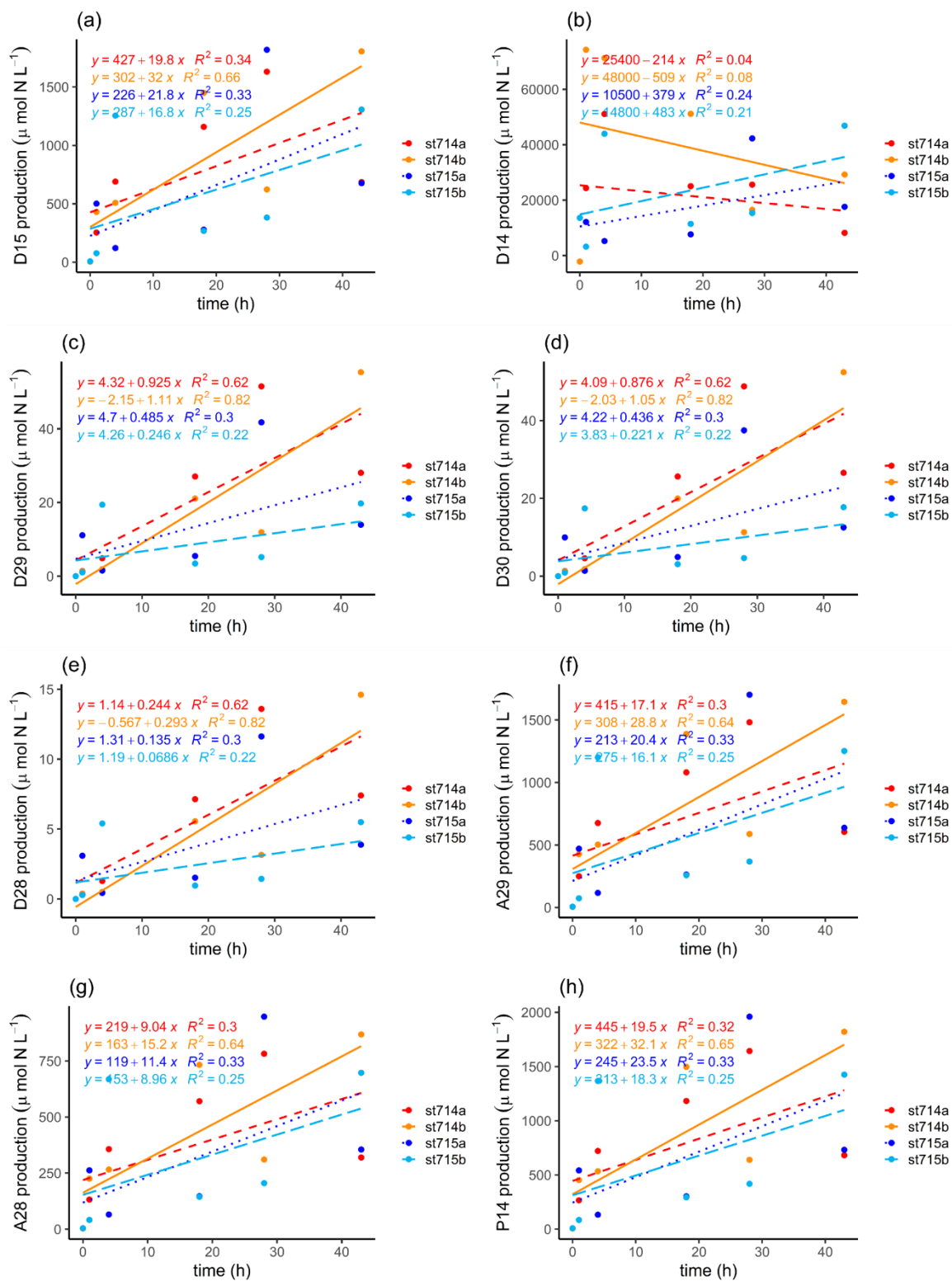
Figure 5. N_2 production during the incubation. N_2 production calculated after Nielsen (1992) of a) added ^{15}N-NO_3^- (D15) and b) in situ ^{14}N-NO_3^- (D14). N_2 production calculated after Risgaard-Petersen et al., (2003) via denitrification of c) $^{29}N_2$ (D29), d) $^{30}N_2$ (D30) e) $^{28}N_2$ (D28), and via anammox of e) $^{29}N_2$ (A29), and f) $^{28}N_2$ (A28). g) Estimation of the genuine ^{14}N-N_2 production (P14) during the incubation after Risgaard-Petersen et al., (2003). Two replicates of each station are given, with station 714a (red dashed) and 714b (orange solid), and station 715a (dark blue dotted) and 715b (light blue long dashed). The slope of the linear regression indicates the production rate of the respective N_2 production as a function of incubation time. Because we only had one initial N_2:Ar ratio for each station, we used this as a start value for the second replicate too.

3.4 TA incubation in BODs

In order to estimate the increase in TA in fluid mud and calculate potential TA generation rates, we used the BOD incubations. In these samples, TA was higher than in surface samples (Fig. 6), with initial concentrations for TA and DIC > 3000 µmol kg^{-1}. During the incubation, we measured increasing TA and DIC concentrations in both stations from the start (0h) to the end (43 h). At station 714, TA increased from 3300 to 3378 µmol TA kg^{-1} and DIC from 3337 to 3435 µmol DIC kg^{-1}. In contrast, station 715 had somewhat lower values with TA increasing from 3168 to 3196 µmol TA kg^{-1} and DIC from 3303 to 3340 µmol DIC kg^{-1}. We used the increasing difference to calculate potential generation rates for station 714 of 1.8 µmol TA kg^{-1} h^{-1} and 2.3 µmol DIC kg^{-1} h^{-1}, and for station 715 of 0.7 µmol TA kg^{-1} h^{-1} and 0.9 µmol DIC kg^{-1} h^{-1} (Table 2).
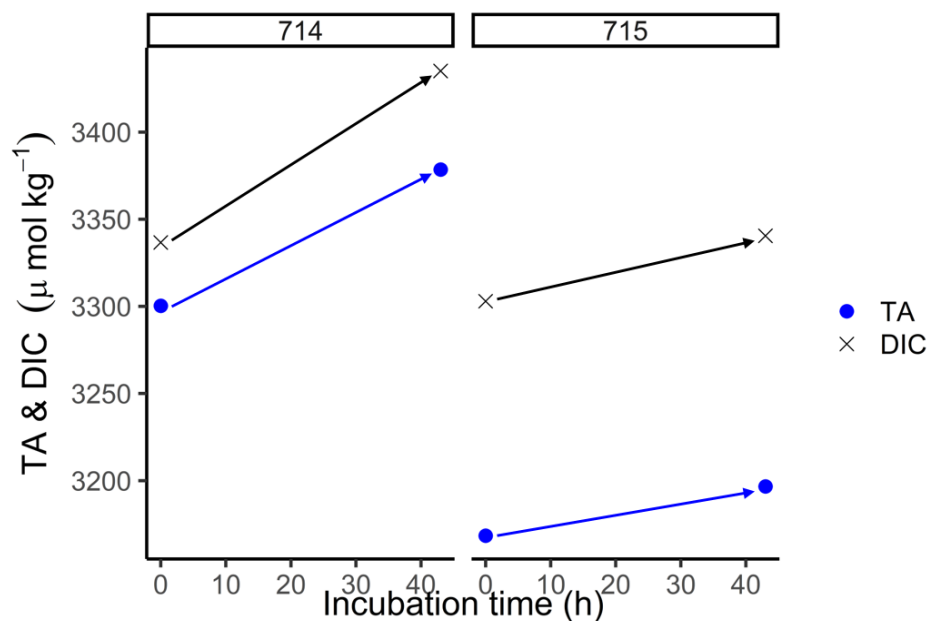
Figure 6. BOD incubations. The start (0h) and end (43h) concentrations of total alkalinity (TA) (blue dots) and dissolved inorganic carbon (DIC) (black crosses) of the BOD incubation samples from station 714 and 715, respectively.

325 **Table 2.** Carbon and Nitrogen values of the incubation experiment. TA generation is the rate of TA generation in the BOD incubation. TA as NO_3^- loss is the consumed NO_3^- that correspond to the amount TA generated (equated with denitrification) recalculated with 0.9. D15 N production is the total produced amount of added $^{15}N\text{-}NO_3^-$ after Nielsen (1992) and calculated as the slope of a linear regression of the produced $^{15}N_2$ concentration as a function of the entire incubation time. Calc. denitrification N production and calc. anammox N production is the estimated amount of added $^{15}N\text{-}NO_3^-$ that was produced by denitrification and anammox, respectively. The estimation based on the

330 approach of combining TA and the N_2 production calculation after Nielsen (1992). We assumed the N_2 produced by anammox as the remaining amount N_2 that was not produced by denitrification. The standard deviation as sample variability is given if possible as ± sd. Average values were calculated of two replicates.

Species	Unit	Station 714	Station 715
TA generation	µmol kg^{-1} h^{-1}	1.8	0.6
TA as NO_3^- loss	µmol L^{-1} h^{-1}	2.0	0.7
Avg. D15 N production ± sd	µmol L^{-1} h^{-1}	25.9 ± 6.1	19.3 ± 2.5
Avg. calc. denitrification N production (D15)	%	7.7	3.5
Avg. calc. anammox N production (D15)	%	92.3	96.5
Avg. calc. denitrification N production (D14)	%	-0.6	0.2
Avg. calc. anammox N production (D14)	%	100.6	99.8

4 Discussion

4.1 TA generation and nitrate respiration in the estuary

335 In comparison to the North Sea with TA and DIC values ranging around 2400 µmol TA kg^{-1} and 2100 µmol DIC kg^{-1} (Thomas et al., 2004), and other German estuaries such as the Elbe Estuary with average values around 2000 µmol kg^{-1} (Amann et al., 2015;Brasse et al., 2002;Norbisrath et al., 2022), the TA and DIC concentrations in the Ems Estuary were clearly higher with values between 2400 µmol kg^{-1} and 2900 µmol kg^{-1}. In particular in the fluid mud, TA and DIC concentrations exceeded the water column concentrations of the Ems Estuary and adjacent zones with values > 3000 µmol kg^{-1}. Thus, the upper Ems

340 Estuary and especially the fluid mud is a clear source of TA, probably driven by anaerobic pathways.

To identify nitrate sinks, nitrate isotopes are frequently used (e.g., Kendall et al., 2007;Middelburg and Nieuwenhuize, 2001;Sigman et al., 2001). According to Kendall et al. (2007), $\delta^{15}N$ values between 15 and 30 ‰ suggest denitrification as the dominant pathway, which is an important sink for anthropogenic nitrate and the global nitrogen budget. In a recent study, Schulz et al. (2022) identified three distinct biogeochemical zones along the Ems Estuary with different predominant nitrogen

345 cycling pathways based on water column properties and stable isotopes. In our focus area, the tidal river, Schulz et al. (2022) found a dominance of denitrification, with nitrification as an additional contributing pathway in the downstream part.

In addition to the assessment along the estuary, we investigated five vertical profiles at Ems stream km 7.2 in the tidal river during ebb tide. They allowed us to scan and detect vertical differences in the water column. The hydrographic properties such as temperature, salinity, and SPM confirmed the clear stratification of the fluid mud in the Ems Estuary.

350 In accordance with the transect data, the observed vertical delta values of nitrate also indicate strong fractionation in all depths supporting denitrification to occur in the water column. The occurrence of denitrification in the water column of the tidal river is also supported by the isotope effects (ε). The isotope effect of $\delta^{15}N$ (34.2 ‰) of VP4 came close to the range for water column denitrification that can vary between 20 and 30 ‰ (Sigman and Casciotti, 2001), the isotope effect of $\delta^{15}N$ (70.2 ‰) of VP5 was very high and exceeded this range by far. While we do not have an explanation for this unexpectedly high isotope

355 effect, it is clear that strong fractionation acts on nitrate isotopes, and denitrification and anammox both are known to coincide with significant effects (Brunner et al., 2013;Casciotti et al., 2003;Granger and Wankel, 2016;Mariotti et al., 1981;Sigman and Casciotti, 2001). Noticeable are the lower $\delta^{18}O$ values in both vertical and horizontal directions, with $\delta^{18}O$ isotope effects of 2.5 ‰ of VP4 and 6.4 ‰ of VP5, respectively. We observed a lower fractionation of $\delta^{18}O$ than $\delta^{15}N$. Interestingly, Dähnke and Thamdrup (2016) found that anammox activity can lead to a decoupling of N and O isotope effects, and that the oxygen

360 isotope effect of nitrate consumption can even be reversed, which matches our findings. Thus, we speculate that the decrease in $\delta^{18}O$ values might point towards anammox activity in the fluid mud.

The observed vertical loss of nitrate revealed a nitrate consumption due to water column denitrification and / or nitrate reduction to nitrite (Fig. 4c). High nitrate concentrations were present during the entire tide and provided sufficient substrate for N_2 producing pathways.

365 Nitrite concentrations increased with depth to maximum concentrations (> 30 µmol L^{-1}) in the deepest layer, which is the intermediate product of either nitrification or denitrification. In the light of decreasing nitrate and oxygen concentrations in the water column, and anoxic conditions in the fluid mud, we rather expect nitrate respiration as the source of nitrite in the deeper layers. In addition, the vertical nitrate loss being higher than nitrite production suggests that nitrite production is fueled by denitrification of nitrate. In order to qualitatively investigate the nitrite sources and support our above results, we used the

370 nitrite stable isotopes. The observed lighter, negative $\delta^{15}N-NO_2^-$ values in the first half during ebb tide point towards nitrification (ammonia oxidation) as source for nitrite, which is an aerobic pathway occurring in the more oxygenated upper water layers during high tide. In contrast, the observed change from the earlier light $\delta^{15}N-NO_2^-$ in the first half during ebb tide to heavy, positive $\delta^{15}N-NO_2^-$ values in the anoxic deeper layers at nearly ebb tide indicates a change in reaction pathways. The heavy, positive $\delta^{15}N-NO_2^-$ values were similar to the observed δ values of nitrate, and are more indicative of nitrate and thus

375 denitrification as the main source of nitrite. This newly produced nitrite is then accessible for either denitrification or anammox. The combination of the high concentrations of nitrite and also ammonium in the deepest layer suggest OM degradation as a potential source of nitrite and ammonium (Blackburn and Henriksen, 1983). The occurrence of such high concentrations of nitrite and ammonium provide sufficient substrate for anammox. The strong stratification of the fluid mud with anoxic conditions facilitates the occurrence of anaerobic N_2 producing pathways in the bottom water of this highly turbid estuary.

380 We further performed an incubation experiment with fluid mud, and were able to discriminate between N_2 production by denitrification and anammox. When calculating N_2 production according to Risgaard-Petersen et al. (2003), we found that more than 90 % of N_2 in the fluid mud at both stations and each time step (Table 2) must originate from anammox (ra).

4.2 TA and N₂ production coupling

The coupling of TA and N_2 production in the tidal river of the Ems Estuary can be used to locate the most active area for TA

385   generation and link part of the increase to water column denitrification. We were also able to identify nitrate / nitrite consumption in the fluid mud and discriminate between denitrification and anammox. In the following, we combined TA generation and nitrate respiration pathways first for the transect surface samples, second for the vertical profiles of the water column, and third for the fluid mud.

Stable nitrate isotopes in surface samples of the present Ems Estuary transect revealed denitrification (Schulz et al., 2022) as

390   the dominant pathway in the inner estuary in the tidal river (weir to Ems stream km 36). The observed denitrification activity matches with the observed increased TA values in this area. However, the general TA gain between upstream the weir and the TA maximum at Ems stream km 7.8, the upper tidal river, was much higher than the concomitant nitrate loss. We assume that parts of the TA gain were generated by denitrification, but that also other metabolic anaerobic pathways or $CaCO_3$ dissolution could generate TA in the water column of the tidal river of the Ems.

395   In the vertical water column profiles, we observed decreasing nitrate concentrations indicating nitrate consumption with depth. In combination with the low oxygen concentrations that also decreased with depth, and the increasing delta values with depth (Fig. 4), we suggest that denitrification appeared in the water column, in particular in the deeper layers, generating TA as a byproduct. The decreasing nitrate and oxygen concentrations and the increasing delta values suggest that high denitrification activity frequently occurred towards the bottom.

400   The fluid mud is indicated by strong vertical gradients of most observed parameters in the deepest 1 m and suggest a strong separation from the upper water column. In particular in the last sampling (VP5), the substantial nitrate consumption resulted in a significant increase of $\delta^{15}N$ values of the remaining nitrate pool. Ongoing denitrification binds H^+ ions, thus increases TA values. We indeed observed higher TA concentrations in the fluid mud than in the water column and suspect that at least some TA is generated by denitrification in the deepest layers.

405   In order to further shed light on the pathways in the fluid mud, we combined the BOD incubation with the N_2 production experiment. Assuming that all TA generation in the BOD incubation containing fluid mud was due to denitrification, which occurred in the deeper layers, we related the TA increase from the BOD incubation to N_2 generation according to Nielsen (1992), and thus estimated N_2 generation by denitrification.

Given a TA generation by denitrification with a ratio of 0.9 (Chen and Wang, 1999), we calculated theoretical denitrification

410   rates based on TA generation and compared the results with total N_2 production of D15 based on Nielsen (1992) (Table 2). We found that a large fraction of N_2 production could not be accounted to denitrification. Based on this mismatch, it appears that 90 % of the N_2 production stems from anammox, which is neutral with regards to TA generation (Middelburg et al., 2020). The dominance of N_2 production by anammox in the fluid mud (90 % N_2 production) is supported by the IPT calculation after Risgaard-Petersen et al. (2003).

415   It is intriguing that we find such a high contribution of anammox in a heterotrophic estuary. Traditionally, anammox has been associated with deep sediments that are poor in organic matter and have low oxygen consumption rates (Dalsgaard et al., 2003;Engström et al., 2005;Kuypers et al., 2003;Thamdrup and Dalsgaard, 2002).

    Other studies that focused on estuarine and coastal regions also found a clear contribution of anammox, albeit in a much lower range. For instance, in the Thamse Estuary (UK), the occurrence of anammox was observed to be much lower with a

420   contribution to N_2 production of < 10 % (Trimmer et al., 2003). Similar low values were observed during summer in the Randers Fjord in Denmark (Risgaard-Petersen et al., 2004), in estuarine and coastal sites in Rhode Island in the USA (Brin et al., 2014), and in the subtropical Logan river in Australia (Meyer et al., 2005). A two times higher maximum contribution of anammox to N_2 production (22 %) was observed by Rich et al. (2008) in Chesapeake Bay, USA.

    But what can be the cause for the dominance of anammox that we find at our study site?

425   Anammox correlates with high concentrations of NO_3^- in the overlying water and high organic carbon content (Nicholls and Trimmer, 2009;Trimmer et al., 2003), which were both present in the tidal river of the Ems Estuary. Dalsgaard et al. (2012) also pointed out the correlation of higher anammox rates at stations with higher ammonium concentrations (close to 5 µmol L^{-1}) and relatively high turbidity in the work of Hamersley et al. (2007) and Lam et al. (2009). In the tidal river of the Ems, and in particular in the fluid mud (Fig. 4), we also observed high concentrations of ammonium, providing sufficient substrate

430   for anammox.

    In addition, the reactivity of the OM can affect anammox (Engström et al., 2005;Trimmer et al., 2003). Engström et al. (2005) identified that in particular fresh and reactive OM favors denitrification, whereas old unreactive OM correlates with higher anammox rates. The reason is probably the difference in maximum growth rates, which favors fast-growing denitrifying bacteria over slow-growing anammox bacteria when available substrate is abundant (You et al., 2020 and references therein).

435   Interestingly, Schulz et al. (2022) found high C:N ratios in this river section, and postulated a low OM reactivity there. Thus, it is plausible that OM in the fluid mud is mostly refractory, because fresh imported OM is already degraded in the water column above the fluid mud, or in the middle reaches of the estuary before reaching the riverine part of the estuary. The DIC excess in relation to TA supports OM degradation (Wang et al., 2016) in the overlying water. This would be in line with the stratification that we found, which separates the fluid mud from the overlying water (Fig. 4). In this case, denitrifier growth

440   and thereby denitrification may be limited by the low reactivity of the OM. This unique niche characterized by high availability of nitrate, nitrite and ammonium, recalcitrant OM, and low oxygen enables anammox to gain importance in the Ems Estuary. We showed that both denitrification and anammox occurred in the deeper layer of the tidal river, but suggest that anammox is the major N_2 producing pathway in the fluid mud.

5 Conclusion

445   In the highly turbid inner Ems Estuary, we observed TA and DIC concentrations being higher than in the North Sea with both values between 2400 and 2900 µmol kg^{-1}, indicating the estuary as a source of TA. Denitrification occurred in the water column

of the tidal river, where we also detected the highest TA concentrations. This led us to assume that denitrification is the source for at least some of the generated TA. However, since the TA gain is much higher than the nitrate loss, we suggest that $CaCO_3$ dissolution or anaerobic pathways other than denitrification could also generate TA in the water column of the tidal river.

450   In the incubation experiment, denitrification rates as identified according to Risgaard-Petersen et al. (2003) were low and anammox contributed > 90 % to potential N_2 production. Based on the assumption that all TA was generated by denitrification in the fluid mud, we were able to discriminate the N_2 production pathways in the high turbidity part of the estuary. Supported by the N_2 production calculations according to Risgaard-Petersen et al. (2003), we were able to show that anammox was the major N_2 production pathway in the fluid mud of the tidal river in the Ems Estuary. Denitrification played a subordinate role

455   and was only relevant in deeper layers of the water column, and denitrification was clearly outcompeted by anammox.

Data availability

The data set of the study by Schulz et al. (2022) is available at https://doi.pangaea.de/10.1594/PANGAEA.942222. The carbon data are in preparation to be released in coastMAP Geoportal (https://www.coastmap.org) connecting to PANGAEA with doi, and are available upon request from the corresponding author.

460   *Acknowledgement*

We thank the crew from RV *Ludwig Prandtl* to enable the cruise, Leon Schmidt for the support during the cruise and the nutrient measurements, and Markus Ankele for the isotope measurements. Thanks to Wasserstraßen- und Schifffahrtsamt Ems-Nordsee for providing the Ems River kilometer data, and Linda Baldewein for helping with river kilometer calculations. This research has been funded by the German Academic Exchange Service (DAAD, project: MOPGA-GRI, grant no. 57429828),

465   which received funds from the German Federal Ministry of Education and Research (BMBF).

Author contribution

MN did the sampling, sample measurement and analyses, the data interpretation and evaluation. AN supported with the MIMS set up, the MIMS data preparation and interpretation. TS & JVB organized the cruise, supported the sampling and data interpretation. JVB did the river sampling at Rhede Brücke and Weir Herbrum. AS did the vertical profile sample collection,

470   measurements, data preparation, and method description. MN, KD, & HT designed this study. MN prepared the manuscript with contribution from all co-authors.

Competing interests

The authors declare that they have no conflict of interest.

References

475 Amann, T., Weiss, A., and Hartmann, J.: Inorganic carbon fluxes in the inner Elbe estuary, Germany, Estuaries and Coasts, 38, 192-210, 2015.

Becker, M., Maushake, C., and Winter, C.: Observations of mud-induced periodic stratification in a hyperturbid estuary, Geophysical Research Letters, 45, 5461-5469, 2018.

Berner, R. A., Lasaga, A. C., and Garrels, R. M.: Carbonate-silicate geochemical cycle and its effect on atmospheric carbon dioxide over
480 the past 100 million years, Am. J. Sci.;(United States), 283, 1983.

Blackburn, T., and Henriksen, K.: Nitrogen cycling in different types of sediments from Danish waters 1, Limnology and Oceanography, 28, 477-493, 1983.

Böhlke, J. K., Smith, R. L., and Hannon, J. E.: Isotopic analysis of N and O in nitrite and nitrate by sequential selective bacterial reduction to N2O, Analytical chemistry, 79, 5888-5895, 2007.

485 Borges, A. V., Delille, B., and Frankignoulle, M.: Budgeting sinks and sources of CO2 in the coastal ocean: Diversity of ecosystems counts, Geophysical research letters, 32, 2005.

Brasse, S., Nellen, M., Seifert, R., and Michaelis, W.: The carbon dioxide system in the Elbe estuary, Biogeochemistry, 59, 25-40, 2002.

Brewer, P. G., and Goldman, J. C.: Alkalinity changes generated by phytoplankton growth 1, Limnology and Oceanography, 21, 108-117, 1976.

490 Brin, L. D., Giblin, A. E., and Rich, J. J.: Environmental controls of anammox and denitrification in southern New England estuarine and shelf sediments, Limnology and Oceanography, 59, 851-860, 2014.

Brunner, B., Contreras, S., Lehmann, M. F., Matantseva, O., Rollog, M., Kalvelage, T., Klockgether, G., Lavik, G., Jetten, M. S., and Kartal, B.: Nitrogen isotope effects induced by anammox bacteria, Proceedings of the National Academy of Sciences, 110, 18994-18999, 2013.

Burt, W., Thomas, H., Hagens, M., Pätsch, J., Clargo, N., Salt, L., Winde, V., and Böttcher, M.: Carbon sources in the North Sea evaluated
495 by means of radium and stable carbon isotope tracers, Limnology and Oceanography, 61, 666-683, 2016.

Casciotti, K. L., Sigman, D. M., Hastings, M. G., Böhlke, J., and Hilkert, A.: Measurement of the oxygen isotopic composition of nitrate in seawater and freshwater using the denitrifier method, Analytical chemistry, 74, 4905-4912, 2002.

Casciotti, K. L., Sigman, D. M., and Ward, B. B.: Linking diversity and stable isotope fractionation in ammonia-oxidizing bacteria, Geomicrobiology Journal, 20, 335-353, 2003.

500 Chen, C. T. A., and Wang, S. L.: Carbon, alkalinity and nutrient budgets on the East China Sea continental shelf, Journal of Geophysical Research: Oceans, 104, 20675-20686, 1999.

Dähnke, K., and Thamdrup, B.: Isotope fractionation and isotope decoupling during anammox and denitrification in marine sediments, Limnology and Oceanography, 61, 610-624, 2016.

Dalsgaard, T., Canfield, D. E., Petersen, J., Thamdrup, B., and Acuña-González, J.: N2 production by the anammox reaction in the anoxic
505 water column of Golfo Dulce, Costa Rica, Nature, 422, 606-608, 2003.

Dalsgaard, T., Thamdrup, B., Farías, L., and Revsbech, N. P.: Anammox and denitrification in the oxygen minimum zone of the eastern South Pacific, Limnology and Oceanography, 57, 1331-1346, 2012.

De Jonge, V. N., Schuttelaars, H. M., van Beusekom, J. E., Talke, S. A., and de Swart, H. E.: The influence of channel deepening on estuarine turbidity levels and dynamics, as exemplified by the Ems estuary, Estuarine, Coastal and Shelf Science, 139, 46-59, 2014.

510 Engström, P., Dalsgaard, T., Hulth, S., and Aller, R. C.: Anaerobic ammonium oxidation by nitrite (anammox): implications for N2 production in coastal marine sediments, Geochimica et Cosmochimica Acta, 69, 2057-2065, 2005.

Frankignoulle, M., Abril, G., Borges, A., Bourge, I., Canon, C., Delille, B., Libert, E., and Théate, J.-M.: Carbon dioxide emission from European estuaries, Science, 282, 434-436, 1998.

Granger, J., and Wankel, S. D.: Isotopic overprinting of nitrification on denitrification as a ubiquitous and unifying feature of environmental
515 nitrogen cycling, Proceedings of the National Academy of Sciences, 113, E6391-E6400, 2016.

Große, F., Greenwood, N., Kreus, M., Lenhart, H.-J., Machoczek, D., Pätsch, J., Salt, L., and Thomas, H.: Looking beyond stratification: a model-based analysis of the biological drivers of oxygen deficiency in the North Sea, Biogeosciences, 13, 2511-2535, 2016.

Hamersley, M. R., Lavik, G., Woebken, D., Rattray, J. E., Lam, P., Hopmans, E. C., Damsté, J. S. S., Krüger, S., Graco, M., and Gutiérrez, D.: Anaerobic ammonium oxidation in the Peruvian oxygen minimum zone, Limnology and Oceanography, 52, 923-933, 2007.

520 Hamme, R. C., and Emerson, S. R.: The solubility of neon, nitrogen and argon in distilled water and seawater, Deep Sea Research Part I: Oceanographic Research Papers, 51, 1517-1528, 2004.

Hansen, H., and Koroleff, F.: Determination of nutrients. Methods of Seawater Analysis: Third, Completely Revised and Extended Edition. Weinheim, Germany: Wiley-VCH Verlag GmbH, 2007.

Howarth, R., Chan, F., Conley, D. J., Garnier, J., Doney, S. C., Marino, R., and Billen, G.: Coupled biogeochemical cycles: eutrophication
525 and hypoxia in temperate estuaries and coastal marine ecosystems, Frontiers in Ecology and the Environment, 9, 18-26, 2011.

Hu, X., and Cai, W. J.: An assessment of ocean margin anaerobic processes on oceanic alkalinity budget, Global Biogeochemical Cycles, 25, 2011.

Jonge, V. d.: Relations between annual dredging activities, suspended matter concentrations, and the development of the tidal regime in the Ems estuary, Canadian Journal of Fisheries and Aquatic Sciences, 40, s289-s300, 1983.

530 Kana, T. M., Darkangelo, C., Hunt, M. D., Oldham, J. B., Bennett, G. E., and Cornwell, J. C.: Membrane inlet mass spectrometer for rapid high-precision determination of N2, O2, and Ar in environmental water samples, Analytical Chemistry, 66, 4166-4170, 1994.

Kendall, C., Elliott, E. M., and Wankel, S. D.: Tracing anthropogenic inputs of nitrogen to ecosystems, Stable isotopes in ecology and environmental science, 2, 375-449, 2007.

Krom, M. D.: Spectrophotometric determination of ammonia: a study of a modified Berthelot reaction using salicylate and dichloroisocyanurate, Analyst, 105, 305-316, 1980.

535 Kroon, H.: Determination of nitrogen in water: comparison of a continuous-flow method with on-line UV digestion with the original Kjeldahl method, Analytica Chimica Acta, 276, 287-293, 1993.

Kuypers, M. M., Sliekers, A. O., Lavik, G., Schmid, M., Jørgensen, B. B., Kuenen, J. G., Sinninghe Damsté, J. S., Strous, M., and Jetten, M. S.: Anaerobic ammonium oxidation by anammox bacteria in the Black Sea, Nature, 422, 608-611, 2003.

540 Lam, P., Lavik, G., Jensen, M. M., van de Vossenberg, J., Schmid, M., Woebken, D., Gutiérrez, D., Amann, R., Jetten, M. S., and Kuypers, M. M.: Revising the nitrogen cycle in the Peruvian oxygen minimum zone, Proceedings of the National Academy of Sciences, 106, 4752-4757, 2009.

Mariotti, A., Germon, J., Hubert, P., Kaiser, P., Letolle, R., Tardieux, A., and Tardieux, P.: Experimental determination of nitrogen kinetic isotope fractionation: some principles; illustration for the denitrification and nitrification processes, Plant and soil, 62, 413-430, 1981.

545 Meybeck, M.: Global chemical weathering of surficial rocks estimated from river dissolved loads, American journal of science, 287, 401-428, 1987.

Meyer, R. L., Risgaard-Petersen, N., and Allen, D. E.: Correlation between anammox activity and microscale distribution of nitrite in a subtropical mangrove sediment, Applied and environmental microbiology, 71, 6142-6149, 2005.

Middelburg, J., and Nieuwenhuize, J.: Nitrogen isotope tracing of dissolved inorganic nitrogen behaviour in tidal estuaries, Estuarine, Coastal 550 and Shelf Science, 53, 385-391, 2001.

Middelburg, J. J., Soetaert, K., and Hagens, M.: Ocean alkalinity, buffering and biogeochemical processes, Reviews of Geophysics, 58, e2019RG000681, 2020.

Mulder, A., Van de Graaf, A. A., Robertson, L., and Kuenen, J.: Anaerobic ammonium oxidation discovered in a denitrifying fluidized bed reactor, FEMS microbiology ecology, 16, 177-183, 1995.

555 Nicholls, J. C., and Trimmer, M.: Widespread occurrence of the anammox reaction in estuarine sediments, Aquatic microbial ecology, 55, 105-113, 2009.

Nielsen, L. P.: Denitrification in sediment determined from nitrogen isotope pairing, FEMS Microbiology Letters, 86, 357-362, 1992.

Nixon, S. W.: Coastal marine eutrophication: a definition, social causes, and future concerns, Ophelia, 41, 199-219, 1995.

Norbisrath, M., Pätsch, J., Dähnke, K., Sanders, T., Schulz, G., van Beusekom, J. E., and Thomas, H.: Metabolic alkalinity release from 560 large port facilities (Hamburg, Germany) and impact on coastal carbon storage, Biogeosciences, 19, 5151-5165, 2022.

Petersen, W., Schroeder, F., and Bockelmann, F.-D.: FerryBox-Application of continuous water quality observations along transects in the North Sea, Ocean Dynamics, 61, 1541-1554, 2011.

Reithmaier, G. M., Ho, D. T., Johnston, S. G., and Maher, D. T.: Mangroves as a source of greenhouse gases to the atmosphere and alkalinity and dissolved carbon to the coastal ocean: A case study from the Everglades National Park, Florida, Journal of Geophysical Research: 565 Biogeosciences, 125, e2020JG005812, 2020.

Rich, J. J., Dale, O. R., Song, B., and Ward, B. B.: Anaerobic ammonium oxidation (anammox) in Chesapeake Bay sediments, Microbial Ecology, 55, 311-320, 2008.

Risgaard-Petersen, N., Meyer, R. L., Schmid, M., Jetten, M. S., Enrich-Prast, A., Rysgaard, S., and Revsbech, N. P.: Anaerobic ammonium oxidation in an estuarine sediment, Aquatic Microbial Ecology, 36, 293-304, 2004.

570 Risgaard-Petersen, N., Nielsen, L. P., Rysgaard, S., Dalsgaard, T., and Meyer, R. L.: Application of the isotope pairing technique in sediments where anammox and denitrification coexist, Limnology and oceanography: methods, 1, 63-73, 2003.

Sanders, T., and Laanbroek, H. J.: The distribution of sediment and water column nitrification potential in the hyper-turbid Ems estuary, Aquatic Sciences, 80, 1-13, 2018.

Schulz, G., Sanders, T., van Beusekom, J. E., Voynova, Y. G., Schöl, A., and Dähnke, K.: Suspended particulate matter drives the spatial 575 segregation of nitrogen turnover along the hyper-turbid Ems estuary, Biogeosciences, 19, 2007-2024, 2022.

Shadwick, E., Thomas, H., Gratton, Y., Leong, D., Moore, S., Papakyriakou, T., and Prowe, A.: Export of Pacific carbon through the Arctic Archipelago to the North Atlantic, Continental Shelf Research, 31, 806-816, 2011.

Sigman, D. M., and Casciotti, K.: Nitrogen isotopes in the ocean, Encyclopedia of ocean sciences, 3, 1884-1894, 2001.

Sigman, D. M., Casciotti, K. L., Andreani, M., Barford, C., Galanter, M., and Böhlke, J.: A bacterial method for the nitrogen isotopic analysis 580 of nitrate in seawater and freshwater, Analytical chemistry, 73, 4145-4153, 2001.

Sigman, D. M., Karsh, K. L., and Casciotti, K. L.: Nitrogen isotopes in the ocean, Encyclopedia of Ocean Sciences (Second Edition), 40-54, https://doi.org/10.1016/B978-012374473-9.00632-9, 2009.

Suchet, P. A., and Probst, J.-L.: Modelling of atmospheric CO2 consumption by chemical weathering of rocks: application to the Garonne, Congo and Amazon basins, Chemical Geology, 107, 205-210, 1993.

585 Talke, S. A., de Swart, H. E., and Schuttelaars, H.: Feedback between residual circulations and sediment distribution in highly turbid estuaries: an analytical model, Continental Shelf Research, 29, 119-135, 2009.

Thamdrup, B., and Dalsgaard, T.: Production of N2 through anaerobic ammonium oxidation coupled to nitrate reduction in marine sediments, Applied and environmental microbiology, 68, 1312-1318, 2002.

Thomas, H., Bozec, Y., Elkalay, K., and De Baar, H. J.: Enhanced open ocean storage of CO2 from shelf sea pumping, Science, 304, 1005-
590 1008, 2004.

Thomas, H., Friederike Prowe, A., van Heuven, S., Bozec, Y., de Baar, H. J., Schiettecatte, L. S., Suykens, K., Koné, M., Borges, A. V., and Lima, I. D.: Rapid decline of the CO2 buffering capacity in the North Sea and implications for the North Atlantic Ocean, Global Biogeochemical Cycles, 21, 2007.

Thomas, H., Schiettecatte, L.-S., Suykens, K., Koné, Y., Shadwick, E., Prowe, A. F., Bozec, Y., de Baar, H. J., and Borges, A.: Enhanced
595 ocean carbon storage from anaerobic alkalinity generation in coastal sediments, Biogeosciences, 6, 267-274, 2009.

Trimmer, M., Nicholls, J. C., and Deflandre, B.: Anaerobic ammonium oxidation measured in sediments along the Thames estuary, United Kingdom, Applied and environmental microbiology, 69, 6447-6454, 2003.

Van Beusekom, J., and De Jonge, V.: Retention of phosphorus and nitrogen in the Ems estuary, Estuaries, 21, 527-539, 1998.

Van Beusekom, J. E., Carstensen, J., Dolch, T., Grage, A., Hofmeister, R., Lenhart, H., Kerimoglu, O., Kolbe, K., Pätsch, J., and Rick, J.:
600 Wadden Sea Eutrophication: long-term trends and regional differences, Frontiers in Marine Science, 370, 2019.

Van Dam, B. R., Zeller, M. A., Lopes, C., Smyth, A. R., Böttcher, M. E., Osburn, C. L., Zimmerman, T., Pröfrock, D., Fourqurean, J. W., and Thomas, H.: Calcification-driven CO2 emissions exceed "Blue Carbon" sequestration in a carbonate seagrass meadow, Science Advances, 7, eabj1372, 2021.

van Maren, D. S., Winterwerp, J. C., and Vroom, J.: Fine sediment transport into the hyper-turbid lower Ems River: the role of channel
605 deepening and sediment-induced drag reduction, Ocean Dynamics, 65, 589-605, 2015.

Voynova, Y. G., Petersen, W., Gehrung, M., Aßmann, S., and King, A. L.: Intertidal regions changing coastal alkalinity: The Wadden Sea-North Sea tidally coupled bioreactor, Limnology and Oceanography, 64, 1135-1149, 2019.

Wang, Z. A., Kroeger, K. D., Ganju, N. K., Gonneea, M. E., and Chu, S. N.: Intertidal salt marshes as an important source of inorganic carbon to the coastal ocean, Limnology and Oceanography, 61, 1916-1931, 2016.

610 Wolf-Gladrow, D. A., Zeebe, R. E., Klaas, C., Körtzinger, A., and Dickson, A. G.: Total alkalinity: The explicit conservative expression and its application to biogeochemical processes, Marine Chemistry, 106, 287-300, 2007.

You, Q.-G., Wang, J.-H., Qi, G.-X., Zhou, Y.-M., Guo, Z.-W., Shen, Y., and Gao, X.: Anammox and partial denitrification coupling: a review, RSC advances, 10, 12554-12572, 2020.